2024 IEEE International Conference on Robotics and Automation (ICRA 2024)
May 13-17, 2024. Yokohama, Japan

Do we need scan-matching in radar odometry?

Vladimír Kubelka, Emil Fritz and Martin Magnusson

***Abstract*— There is a current increase in the development of "4D" Doppler-capable radar and lidar range sensors that produce 3D point clouds where all points also have information about the radial velocity relative to the sensor. 4D radars in particular are interesting for object perception and navigation in low-visibility conditions (dust, smoke) where lidars and cameras typically fail. With the advent of high-resolution Doppler-capable radars comes the possibility of estimating odometry from single point clouds, foregoing the need for scan registration which is error-prone in feature-sparse field environments. We compare several odometry estimation methods, from direct integration of Doppler/IMU data and Kalman filter sensor fusion to 3D scan-to-scan and scan-to-map registration, on three datasets with data from two recent 4D radars and two IMUs. Surprisingly, our results show that the odometry from Doppler and IMU data alone give similar or better results than 3D point cloud registration. In our experiments, the position drift can be as low as 0.9% over 1.8 and 4.5 km trajectories. That allows accurate estimation of 6-DOF ego-motion over long distances also in feature-sparse mine environments. These results are useful not least for applications of navigation with resource-constrained robot platforms in feature-sparse and low-visibility conditions such as mining, construction, and search & rescue operations.**

***Index Terms*— 4D Radar, Radar Odometry, Mobile robot, Localization**

I. Introduction

Rapid development in millimeter wave imaging radars, driven by the automotive industry, has enabled localization and mapping in environments where we expect deteriorated visibility conditions and dirt deposition on the sensors. Deploying autonomous vehicles in the mining industry, construction or search & rescue are example applications that demand such capability. Modern imaging radars, similarly to 3D lidars, provide 3D scans of the surroundings. They are additionally able to estimate the radial velocity of each sensed 3D point by leveraging precise phase measurements of the returning signal. This Doppler velocity, as we further denote it, has proven to be advantageous for odometry methods, aiding in the segmentation of dynamic and static objects [1], as well as introducing more constraints to the ego-motion estimation [2], [3]. Moreover, the velocity measurement comes without the need to perform data association, which can be challenging in feature-sparse environments, such as underground mines. Such advantage motivates innovations even in the lidar field in the form of Doppler-capable lidars [4].

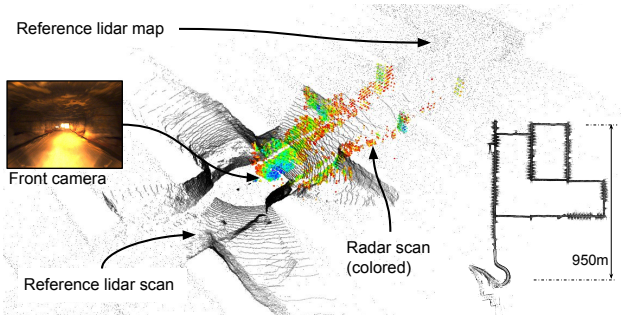

Fig. 1: Detail from the Kvarntorp mine environment captured by two sensor modalities, lidar and radar. The radar modality suffers from limited field of view (FOV), lower resolution and fewer returns. It is however more suitable for low-visibility conditions expected in mining.

In recent years, several approaches to radar odometry and simultaneous localization and mapping (SLAM) have emerged. Motivated by the problem of developing a SLAM system for an underground mining environment, we compare several representative radar odometry estimation methods. To that end, we deploy them on three datasets that include two distinct modern imaging radars. Two datasets have been recorded with our mobile sensor rig: in an underground mine (Fig. 1) and in an outdoor testing site for large wheel loaders (Figs. 3 and 4). The third dataset has been published by Zhang et al. [5] and represents a structured urban environment. Surprisingly, using the simplest method of directly fusing the Doppler-based radar ego-velocity with the orientation provided by an inertial measurement unit (IMU), we are able to achieve localization drift as low as 0.9% over 1.8 km and 4.5 km trajectories from the outdoor testing site and the mine. We find this experimental result useful for designing localization and mapping systems for the mentioned applications and worth spreading in the robotics community for further investigation. Moreover, we make our dataset publicly available at `https://github.com/kubelvla/mine-and-forest-radar-dataset` as the high-grade radars are still difficult to obtain.

II. Related Work

Classical 2D scanning radars usually provide the scans in the form of *spectral images*, which encode signal intensity in the radial direction for every azimuth they measure. Cen et al. [6], [7] proposed methods to extract radar key points from such spectral images and showed how their approach improves the scan matching. Later works such as Barnes et

This work was supported by Sweden's Innovation Agency under grant number 2021-04714 (Radarize). The authors would also like to express their gratitude to Annika Nilsson for her part in the implementation and experimental evaluation of this work.

Vladimír Kubelka (`vladimir.kubelka@oru.se`) and Martin Magnusson (`martin.magnusson@oru.se`) are with the MRO lab of the AASS research centre at Örebro University, Sweden. Emil Fritz is with Örebro University, Sweden.

al. [8] include machine-learning techniques to improve the key point detection. Burnett et al. [9] shows the importance of addressing motion distortion and Doppler shift in the radar data. Contrary to searching for key points, Adolfsson et al. [10] approach the problem from the point cloud perspective, focusing on local geometry. Park et al. [11] avoid point matching altogether by applying Fourier-Mellin transform to find correlation between subsequent radar scans.

The rapid development of 4D Doppler-capable imaging radars opens new possibilities in object detection, motion estimation and localization. The surveys by Venon et al. [12] and Zhou et al. [13] provide comprehensive overview of the state of the art in this research direction. The mmWave sensors by Texas Instruments have gained a lot of attention, as they are lightweight and still provide tens of 3D points with Doppler velocity. Doer and Trommer [2] propose a loosely-coupled extended Kalman filter (EKF) filtering method, which fuses radar ego-velocity, inertial and barometric measurements to track the pose of an unmanned aerial vehicle (UAV). They develop a RANSAC-based least squares optimization algorithm to extract the radar ego-velocity from the radar data. In their later work [14], they incorporate global navigation satellite system (GNSS) measurements as well. In our work, we adopt their open-source implementation to perform experiments with our sensor suite. Contrary to a filtering approach, Kramer et al. [15] propose a sliding window optimization algorithm that fuses Doppler and inertial measurements to track a pose of a mobile sensor rig. They verify their results in underground and outdoor environments. The work of Ng et al [16] extends this approach by choosing a continuous-time trajectory representation that avoids the problems related to synchronization of multiple concurrently running radars. Focusing on the UAV application, Michalczyk et al. [3], [17] propose a tightly-coupled, EKF-based radar odometry. Their approach includes point matching, where the perceieved distance between the matched points, together with the Doppler velocity, serves as the residual vector for the EKF. Lu et al. [18] takes a different direction, both radar measurements and inertial measurement are processed by a deep neural network (DNN) to estimate pose of a mobile agent.

As the 4D imaging radars evolve and their resolution increases, classical 3D scan-matching methods have become feasible. Zhuang et al. [19] fuse inertial data, Doppler-based ego-motion estimates and scan-to-submap constraints by an iterative EKF to obtain radar odometry. In a separate module, they complete the system into a full SLAM solution by performing a generalized ICP (GICP)-based loop closure and global map optimization. They use a Continental ARS548 radar with $300\,\mathrm{m}$ range and $0.3\,\mathrm{m}$ resolution that produces approximately 400 points per scan. Zhang et al. [5] choose a classical SLAM approach with their Oculii Eagle radar sensor (approximately 5000 points per scan in their public dataset). They modify the SLAM network from Koide et al. [20] by adding a modified GICP matching algorithm that takes into account the specific spatial uncertainties in radar point clouds. Since their work and dataset are open-source, we include them in our experimental evaluation.

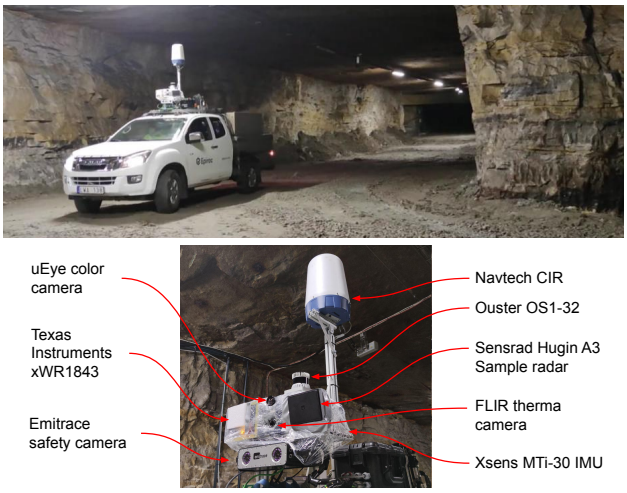

Fig. 2: The pick-up truck driving through the Mine with the multi-sensor rig attached to the roof (top). The sensor rig detail (bottom).

Fig. 3: Aerial view of the Forest environment (left, source: Google Maps©) and the Volvo CE wheel loader equipped with the sensor rig (right).

III. Radar Odometry Variants

From the variety of radar odometry methods, we choose a set which is available open-source, applicable to our sensors and spans from simple sensor fusion to advanced scan-matching.

A. Doppler velocity and IMU

The simplest approach to pose estimation tested in this work exploits the orientation provided by an IMU and ego-velocity as measured by a Doppler-capable radar sensor. The ego-velocity is first transformed from the coordinate frame of the moving platform to the world coordinate frame based on the IMU attitude. It is then numerically integrated assuming constant velocity between consecutive radar scans. This way, a trajectory expressed in the world coordinate frame is generated. Further in the text, we refer to this approach as to *IMU+Doppler*.

Since the radar does not directly provide the ego-velocity measurement but rather radial components of its detected target velocities, it is necessary to robustly process this information to estimate the ego-velocity of the radar. For this purpose, we deploy the approach and implementation[1]

[1] https://github.com/christopherdoer/reve

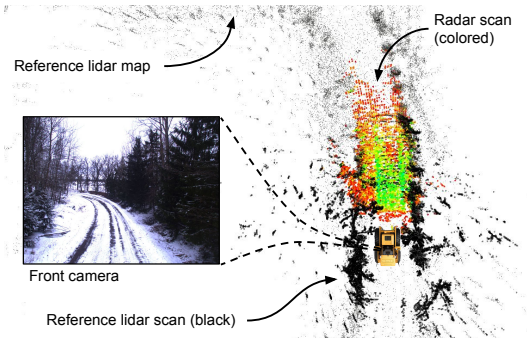

Fig. 4: Top-view of a yellow wheel loader navigating a forest road. From its suite of sensors, lidar, radar and front camera are shown. The dark black points denote the active lidar scan, which is in contrast with the colored, front-facing radar scan.

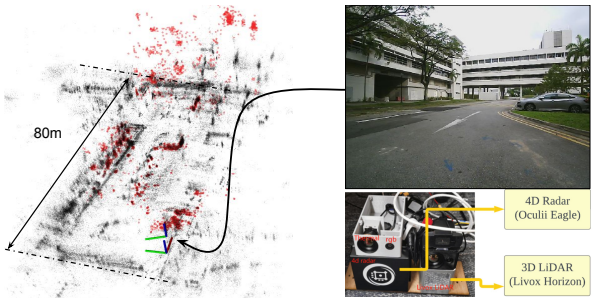

Fig. 5: Assembled radar map of the Car Park environment (left) denoted by black points with a live radar scan (red points). The sensor rig (bottom right) was manually pushed along the trajectory. The data and figures adopted from [5].

by Doer and Trommer [2]. Their *3-Point RANSAC-LSQ* ego-motion estimation method applies RANSAC to the underlying least squares optimization problem (eq. 27–32 in [2]). This algorithm is highly efficient. The average processing time for one radar scan is $10\,\mathrm{ms}$ in our dataset.

B. Extended Kalman Filter fusion

In contrast to direct Doppler+IMU fusion, employing the EKF allows more principled handling of noise in the sensor measurements and provides pose confidence estimates. We benefit from the implementation[2] by Doer and Trommer [2] which combines their 3-Point RANSAC-LSQ ego-motion estimation with inertial and barometric measurements. The sensor measurements are fused in a loosely-coupled manner by an EKF. From several extensions of the algorithm available, we choose the original *ekf-rio* version. It does not require a radar trigger signal, which we unfortunately do not get from our radar. The algorithm applies, in that case, the incoming ego-motion measurements with a lag of approximately $100\,\mathrm{ms}$ which can impede the state estimation quality, especially during highly dynamical motion. Moreover, we omit the barometer measurements as our sensor rig lacks this sensor. The results we obtain here therefore represent a lower bound on the odometry quality achievable by the filtering methods. We refer to this approach as to EKF in the following text.

[2]https://github.com/christopherdoer/rio

It is noteworthy that the works of Michalczyk et al. [3], [17] report improvements upon [2] by employing a tightly-coupled EKF filtering for radar-inertial odometry. They are able to achieve localization drift below 1%. It remains an interesting question how the tightly-coupled algorithm handles the high-grade radar scans of thousands of targets.

C. Point-to-plane Iterative Closest Point with local map

The high resolution of the tested radars allow us to test methods originally developed for registration of lidar point clouds. For testing the scan-to-submap matching variant, we use the *norlab-icp-mapper*[3] which is open-source and highly configurable. It supports a range of iterative closest point (ICP) variants, from which we choose the *point-to-plane* variant as it generally performs well in structured and semi-structured environments. This mapper does not support map optimization by loop closure identification, it rather builds a monolithic map and thus behaves as a lidar odometry method. The mapper is set to add new points into the map up to a maximum density defined by the minimum distance between points, which is $0.1\,\mathrm{m}$ in our case. Point-to-plane ICP also requires estimation of normal vectors based on local geometry around each point in the map, we use 15 nearest points for that. Also, this mapper requires a prior motion estimate when deployed on the radar data. We thus provide the Doppler+IMU pose as the prior in all experiments.

The ICP algorithm in the mapper offers full 6-degrees of freedom (DOF) pose estimation, or a constrained 4-DOF pose estimation. In the 4-DOF variant, only position and heading are optimized in the point cloud registration, the other two DOF are directly adopted by the mapper from the IMU-provided orientation. In this work, we test both variants, and refer to them as to *ICP* and *ICP 4DOF*.

D. Scan-to-scan matching variants

The final group of radar odometry variants tested in this work employs the scan-to-scan matching, which is often used in front-end modules of larger SLAM frameworks. Zhang et al. [5] successfully applies this approach in a SLAM framework with a modern imaging radar (Oculii Eagle). Since their implementation of the SLAM framework is open-source[4], we include it here for testing their radar odometry with our radar dataset. Moreover, they provide one session from their dataset which in turn allows us to test all the other approaches with the Oculii Eagle radar. Their radar odometry front-end is highly configurable, allowing users to choose from several other scan-matching algorithms. We choose to test their adaptive probability distribution-GICP (APDGICP) variant of GICP. Their scan-matching method can function without a prior motion estimate, yet we modify the code to include the option to use the Doppler+IMU odometry prior. This makes the comparison with the scan-to-submap-matching variants fair. When providing the prior, we

[3]https://github.com/norlab-ulaval/norlab_icp_mapper

[4]https://github.com/zhuge2333/4DRadarSLAM

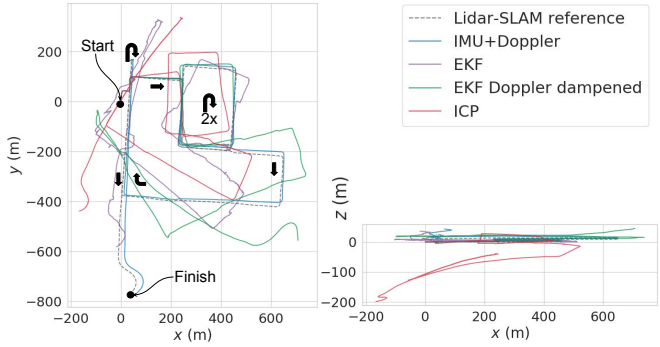

Fig. 6: The Mine environment recorded with the Sensrad Hugin radar. The ICP 4DOF is omitted from this plot for clarity, its vertical drift would be limited compared to the standard ICP shown in red. Similarly, the scan-to-scan matching odometries are not shown for their fast divergence.

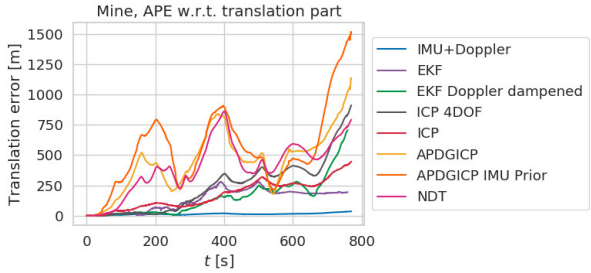

Fig. 7: The translation component of APE in the Mine for all discussed odometry variants.

refer to the method as to *APDGICP IMU Prior*, *APDGICP* otherwise.

We also choose to test their implementation of the normal distributions transform (NDT) scan-matching algorithm as it is often used in lidar odometry solutions. For NDT, we always use the Doppler+IMU prior and refer to it as to *NDT* in the evaluation.

IV. Experiments and Analysis

This section first introduces the two environments and sensors used for recording the experimental trajectories and then one experiment adopted from the dataset published by Zhang [5]. Subsequently, the odometry performance is studied by the means of the absolute pose error (APE), relative pose error (RPE) [21], and the KITTI metrics [22].

A. Environment and sensor setup

Motivated by research towards SLAM in harsh environmental conditions, two field datasets were recorded: one in

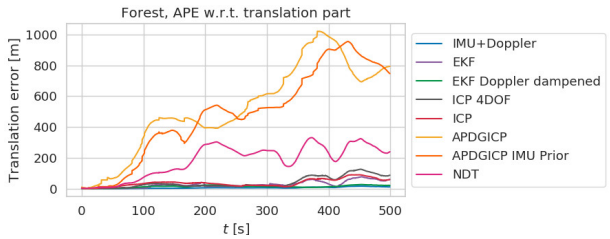

Fig. 8: The translation component of APE in the Forest for all discussed odometry variants.

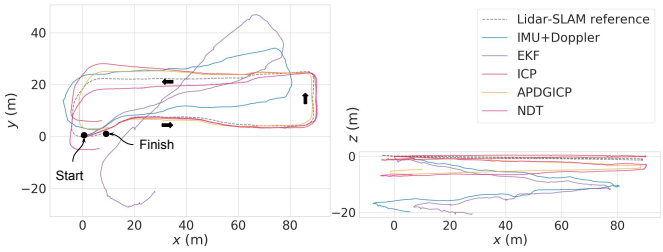

Fig. 9: The Car Park experiment from [5] recorded with the Oculii Eagle radar. Only selected odometry variants shown for better clarity.

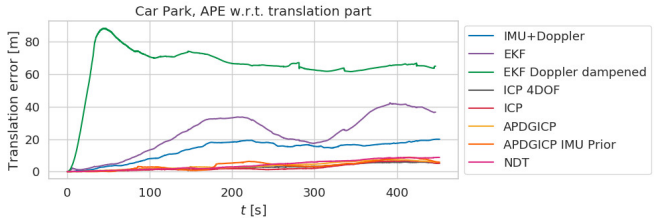

Fig. 10: The APE values for the Car Park environment for all discussed odometry variants.

the Kvarntorp research mine outside of Örebro, Sweden, and one at an outdoor testing site for Volvo Construction Equipment wheel loaders and dumpers in Eskilstuna, Sweden.

The Kvarntorp test mine provides a model environment for underground mining applications. A $4500\,\mathrm{m}$-long run was recorded with a sensor rig attached to the roof of a pick-up truck as shown in Fig. 2. The average speed was $21\,\mathrm{km\,h^{-1}}$ which is close to the max safely drivable speed in the mine. Fig. 1 gives a general impression of the tunnels. At some locations, the tunnels are straight with no side-tunnels and these sections are generally the most demanding for any kind of SLAM, regardless the modality. On the other hand, locations with side-tunnels provide a large number of geometrical constraints beneficial for SLAM algorithms. Fig. 1 shows such an area with two modalities: lidar in greyscale points and radar in colored points. For reference, the view from an RGB camera is also provided. Further in the text, we refer to this experiment as *Mine*.

The Eskilstuna outdoor testing site (further referred to as *Forest*) is used by Volvo CE for development and testing of their products, including the large wheel loaders as shown in Fig. 3. For our experiments, the sensor rig used in Mine was moved from the pickup truck to the Volvo wheel loader. A $1800\,\mathrm{m}$-long loop trajectory through open space and on a forest road (see Fig. 4) was recorded. It was repeated twice, with the average speed of $13.6\,\mathrm{km\,h^{-1}}$. Real-time kinematic positioning (RTK) reference was recorded but for the purposes of this study, we base our metrics on a lidar-SLAM-based reference, which provides the full 6-DOF pose. The median value of the difference between the RTK and the lidar SLAM poses is $1.2\,\mathrm{m}$, mainly due to lower quality of the RTK localization close to trees. Further details including the RTK quality statistics are provided in the dataset.

The sensor suite used in the experiments is detailed in Fig. 2. The sensors are attached to a metal rig and connected

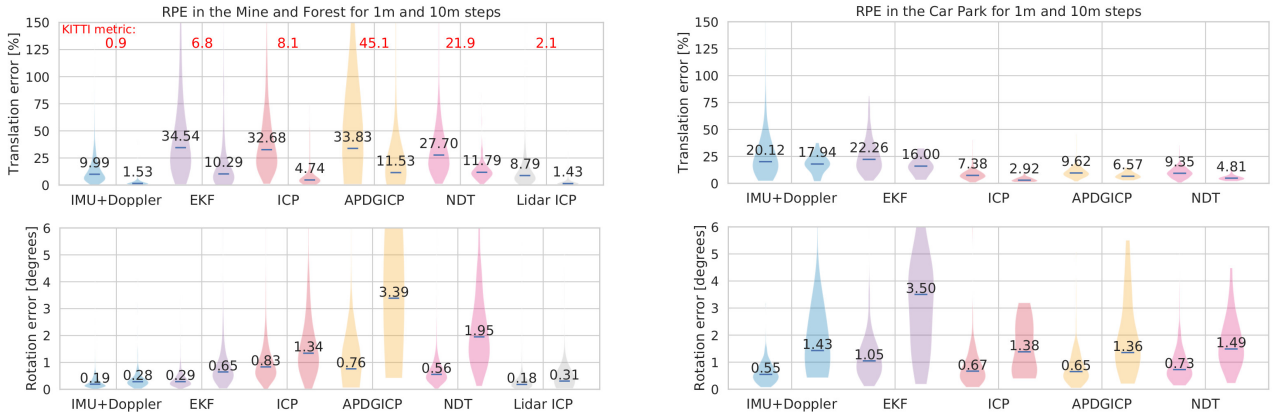

Fig. 11: RPE values for the two distinct sensor setups. Each pair of the violin plots represents the step sizes for evaluating RPE, $1\,\mathrm{m}$ and $10\,\mathrm{m}$ respectively. The median RPE value is shown directly in each plot. Additionally, the Forest and Mine evaluation includes the KITTI translation error metric.

to an Intel NUC computer that runs Ubuntu with ROS and saves raw data as ROS bag files. The suite consists of three radars, one lidar, three cameras and an IMU. The radar used in Mine and Forest is the Sensrad Hugin A3 radar, with horizontal and vertical FOV $80°$ and $30°$ respectively. Thanks to its configuration of 48×48 transmitting and receiving antennas, the horizontal and vertical resolution is $1.25°$ and $1.7°$. The radar is operated in *short range* settings, which implies maximum range $42\,\mathrm{m}$, but grants the highest range resolution of $0.1\,\mathrm{m}$. The frame rate is $16\,\mathrm{Hz}$ with approximately 10000 points per scan. For reference localization, an Ouster OS1-64 lidar is used with the frame rate of $10\,\mathrm{Hz}$ and PTP time-stamping. Finally, inertial data come from Xsens MTi-30 IMU at $400\,\mathrm{Hz}$ rate. The IMU is running its own attitude estimation using the *VRU General* profile, which does not use magnetometer data to absolutely reference the heading angle. Yet, the magnetometer measurements are still used to estimate gyro biases and thus limit the heading drift down to $3\,^\circ\,\mathrm{h}^{-1}$ in ideal conditions.

The Car Park trajectory is a part of the dataset recorded by Zhang et al. [5]. In their setup, they used the Oculii Eagle radar that provides FOV of $120° \times 30°$ (horizontal, vertical) and resolution of $0.5°$, $1°$ and $0.16\,\mathrm{m}$ (horizontal, vertical, range). In the Car Park experiment, the radar scans contain approximately 5000 points. The range of the sensor is over $350\,\mathrm{m}$ and the manufacturer indicates that adaptive modulation is used to boost resolution while maintaining long range. From the point clouds provided in the dataset, it is apparent that some enhancement is applied by the sensor software. Zhang's sensor rig, shown in Fig. 5, also includes a lidar, barometer, camera and two IMUs, a standalone Vectornav VN-100 IMU and an internal IMU of the lidar sensor. For testing the odometry variants that require inertial data, we use the Vectornav IMU measurements. The trajectory of the Car Park experiment is a rectangle recorded by a hand-pushed trolley with the sensor rig attached to it. The environment is a parking lot between buildings at a university campus. The pre-computed ground-truth localization based on a lidar SLAM solution is available in the dataset and used by us.

B. Odometry performance evaluation

To compare the performance of the radar odometry variants presented in Section III, we use the widely adopted APE and RPE metrics, in the *Evo* library implementation [21]. APE together with trajectory plots provides the initial, general idea about the odometry variant behavior for the given sensory and environmental combinations, but is susceptible to the multiplicative, nonlinear effect of the accumulated attitude error. RPE complements this metric, with the indication of the rate of error accumulation. For APE, we provide its translation component, as the rotation error is apparent in the accompanying trajectory plots. For RPE, we show an overall statistic for both components. Moreover, the Mine and Forest are long enough for the KITTI-style [22] error metric. This average relative position error over 100, 200, ..., $800\,\mathrm{m}$ segments is widely used and puts the results into context with other studies. The ground-truth poses for evaluating the odometry error come from lidar-based SLAM. The lidar map and the reference localization was created by the open-source *HDL Graph Slam* [20] implementation supported by a radar prior, see the dataset for details.

Fig. 6 and Fig. 7 demonstrate the perfomance of the discussed radar odometries in the Mine experiment. The scan-to-scan matching APDGICP variants (with and without our prior provided) together with NDT are not suitable for the type of output the Hugin radar provides. We omit them from the Fig. 6 plot since they randomly diverge, as can be seen in the APE plot. We attribute this to the low density and high variance in subsequent radar scans, which causes the scan-to-scan matching approach to quickly diverge. This behavior is similar also in the case when we provide the more accurate IMU+Doppler prior estimate. The main source of error, as we later show in RPE, is the strong drift in attitude.

The scan-to-submap matching represented by the ICP variants (4-DOF and 6-DOF) performs better in the Mine experiment, although the drift is much stronger compared to what would be expected with lidar odometry in similar

environments (e.g., refer to the SLAM results of the Subterranean DARPA robotic challenge [23]). Constraining the ICP to four DOF reduces the vertical drift and results in overall lower APE.

Comparable results are obtained from the EKF approach, which is free from the scan-matching problems, but suffers from abrupt changes in the measured Doppler velocity. As long as the ground is smooth, the localization drift is comparable to lidar odometry drift rates, i.e. approximately 1%. Once the truck hits a bump, the EKF reacts by inappropriate corrections, which can be observed at 180 and 250 seconds in the Mine experiment. As the Hugin radar does not provide a measurement trigger signal, we assume that the measurement lag causes mismatch with the inertial measurements. The radar scans are time-stamped, however the available EKF implementation does not recompute the past states, it rather counts on timely trigger signals and the *state cloning* technique. This problem can be partially alleviated by increasing the measurement uncertainty in the Doppler velocity, which makes the estimated trajectory smoother, but also reduces the EKF capacity to quickly estimate sensor biases and to sense minor motions. We denote this altered variant as *Doppler dampened* in the plots.

Surprisingly, the simplest IMU+Doppler approach shows the best results. The drift is minimal, comparable to the best state-of-the-art lidar odometry techniques. We attribute this to the high accuracy of the Hugin radar in the Doppler velocity values, and to the capability of the particular IMU unit to suppress the heading drift by benefiting from the magnetometer measurements. The downside is that it does not, contrary to the other techniques, provide any confidence estimate.

The results from the Forest experiment follow the trend of the Mine experiment. Fig. 8 shows that the scan-to-scan techniques diverge immediately and the scan-to-submap ICP drifts with similar rate compared to the Mine experiment. The main difference is in the behavior of the Doppler dampened EKF. Thanks to the slower pace and the overall stability of the large and heavy wheel loader, it does not suffer from the abrupt Doppler velocity jolts and closely follows the simple IMU+Doppler odometry.

In the Car Park experiment with the Oculii Eagle radar, we see a different trend. Fig. 9 shows that the simpler methods, i.e. IMU+Doppler and EKF, suffer from vertical and heading drift. We assume that this is mainly due to the type of IMU used by [5] when recording the dataset. The Doppler dampened EKF is omitted from the trajectory plot because it immediately diverges due to accelerometer bias, which takes a minute to estimate (see Fig. 10). Moreover, the Doppler velocity estimation is less accurate in this dataset, which affects the smoothness of the trajectory. We assume that the scan enhancement process inside the sensor may affect the quality of the Doppler velocity values. On the other hand, all the scan-matching techniques perform well. The longer range and the adaptive modulation in the Eagle radar make the the task of scan matching more reliable. In fact, all variants of ICP, APDGICP and NDT perform similarly and stay within $10\,\mathrm{m}$ in APE as shown in Fig. 10.

We summarize the performance of the odometry methods with the two distinct radars in Fig. 11 using the RPE metric. For clarity, we omit the sub-variants in this plot as their RPE does not differ substantially. The trajectories are divided into $1\,\mathrm{m}$ and $10\,\mathrm{m}$ steps for the RPE evaluation. The plot shows the distribution of the translation and rotation errors with the median value directly in the plot. The translation error is expressed as percentage of the step, the rotation error is left in the absolute value, therefore the longer steps yield larger rotational error. Also note that in translation, we observe higher relative errors in the $1\,\mathrm{m}$ steps. Given the already high accuracy of all the methods, we are approaching the noise in the ground-truth localization based on the lidar SLAM. This is also why we do not consider single-frame-sized steps, for which more accurate reference would be necessary.

The Mine and Forest experiments with the Hugin radar are mainly affected by the noise in the estimated attitude, as the translation error differences between the methods are not as profound as the resulting APE. The rotation part of the RPE metric confirms the trend seen in APE. The raw orientation provided by the Xsens IMU supports the highly accurate Doppler velocity and leads to the highly accurate results. For reference, we also provide lidar odometry RPE based on the 64-beam Ouster sensor. The *norlab-icp-mapper* is running 6-DOF pose estimation with the IMU+Doppler prior, local map and no loop closure.

The Car Park experiment reveals that the translation is worse for the methods depending on the Doppler velocity (IMU+Doppler, EKF). In the rotation errors, we see the limiting effect of the scan matching, which prevents larger errors to accumulate, contrary to IMU+Doppler and EKF.

V. CONCLUSIONS

In this work, we have compared several radar odometry methods on three datasets recorded in underground and outdoor environments with two distinct modern imaging radars. With the Oculii Eagle radar, the scan-matching methods achieved higher accuracy than the filtering methods. On the other hand, thanks to the accurate industrial-grade IMU and the Hugin radar, the simplest sensor fusion method IMU+Doppler achieves only 0.9% position drift (KITTI metric) in the Mine and Forest experiments. Provided additional confidence estimation, this method would be suitable for resource-constrained machines operating in harsh environments, such as heavy machinery in the mining industry.

Do we need scan-matching in radar odometry, then? We argue that with the combination of industrial-grade sensors presented here, the scan-matching step can be omitted. The accuracy is comparable to lidar odometry and sufficient for SLAM applications. On the other hand, the additional geometric information leveraged by scan-matching is still necessary when using consumer-grade IMUs or when encountering noisy Doppler velocity measurements. In any case, scan-matching remains necessary for loop-closure identification and localization in already-built maps as any odometry method bears some non-zero localization drift.

REFERENCES

[1] A. Kingery and D. Song, "Improving ego-velocity estimation of low-cost Doppler radars for vehicles," *IEEE Robotics and Automation Letters*, vol. 7, no. 4, pp. 9445–9452, 2022.

[2] C. Doer and G. F. Trommer, "An EKF based approach to radar inertial odometry," in *2020 IEEE International Conference on Multisensor Fusion and Integration for Intelligent Systems (MFI)*, 2020, pp. 152–159.

[3] J. Michalczyk, R. Jung, and S. Weiss, "Tightly-coupled ekf-based radar-inertial odometry," in *2022 IEEE/RSJ International Conference on Intelligent Robots and Systems (IROS)*, 2022, pp. 12 336–12 343.

[4] D. J. Yoon, K. Burnett, J. Laconte, Y. Chen, H. Vhavle, S. Kammel, J. Reuther, and T. D. Barfoot, "Need for speed: Fast correspondence-free lidar-inertial odometry using doppler velocity," in *2023 IEEE/RSJ International Conference on Intelligent Robots and Systems (IROS)*, 2023, pp. 5304–5310.

[5] J. Zhang, H. Zhuge, Z. Wu, G. Peng, M. Wen, Y. Liu, and D. Wang, "4dradarslam: A 4d imaging radar slam system for large-scale environments based on pose graph optimization," in *2023 IEEE International Conference on Robotics and Automation (ICRA)*, 2023, pp. 8333–8340.

[6] S. H. Cen and P. Newman, "Precise ego-motion estimation with millimeter-wave radar under diverse and challenging conditions," in *2018 IEEE International Conference on Robotics and Automation (ICRA)*, 2018, pp. 6045–6052.

[7] S. H. Cen and P. Newman, "Radar-only ego-motion estimation in difficult settings via graph matching," in *2019 International Conference on Robotics and Automation (ICRA)*, 2019, pp. 298–304.

[8] D. Barnes and I. Posner, "Under the radar: Learning to predict robust keypoints for odometry estimation and metric localisation in radar," in *2020 IEEE International Conference on Robotics and Automation (ICRA)*, 2020, pp. 9484–9490.

[9] K. Burnett, A. P. Schoellig, and T. D. Barfoot, "Do we need to compensate for motion distortion and Doppler effects in spinning radar navigation?" *IEEE Robotics and Automation Letters*, vol. 6, no. 2, pp. 771–778, 2021.

[10] D. Adolfsson, M. Magnusson, A. Alhashimi, A. J. Lilienthal, and H. Andreasson, "Cfear radarodometry-conservative filtering for efficient and accurate radar odometry," in *2021 IEEE/RSJ International Conference on Intelligent Robots and Systems (IROS)*. IEEE, 2021, pp. 5462–5469.

[11] Y. S. Park, Y.-S. Shin, and A. Kim, "PhaRaO: Direct radar odometry using phase correlation," in *2020 IEEE International Conference on Robotics and Automation (ICRA)*. IEEE, 2020, pp. 2617–2623.

[12] A. Venon, Y. Dupuis, P. Vasseur, and P. Merriaux, "Millimeter wave fmcw radars for perception, recognition and localization in automotive applications: A survey," *IEEE Transactions on Intelligent Vehicles*, vol. 7, no. 3, pp. 533–555, 2022.

[13] Y. Zhou, L. Liu, H. Zhao, M. López-Benítez, L. Yu, and Y. Yue, "Towards deep radar perception for autonomous driving: Datasets, methods, and challenges," *Sensors*, vol. 22, no. 11, 2022. [Online]. Available: https://www.mdpi.com/1424-8220/22/11/4208

[14] C. Doer, J. Atman, and G. F. Trnmmer, "Gnss aided radar inertial odometry for uas flights in challenging conditions," in *2022 IEEE Aerospace Conference (AERO)*, 2022, pp. 1–10.

[15] A. Kramer, C. Stahoviak, A. Santamaria-Navarro, A.-A. Agha-Mohammadi, and C. Heckman, "Radar-inertial ego-velocity estimation for visually degraded environments," in *2020 IEEE International Conference on Robotics and Automation (ICRA)*. IEEE, 2020, pp. 5739–5746.

[16] Y. Z. Ng, B. Choi, R. Tan, and L. Heng, "Continuous-time radar-inertial odometry for automotive radars," in *2021 IEEE/RSJ International Conference on Intelligent Robots and Systems (IROS)*, 2021, pp. 323–330.

[17] J. Michalczyk, R. Jung, C. Brommer, and S. Weiss, "Multi-state tightly-coupled ekf-based radar-inertial odometry with persistent landmarks," in *2023 IEEE International Conference on Robotics and Automation (ICRA)*, 2023, pp. 4011–4017.

[18] C. X. Lu, M. R. U. Saputra, P. Zhao, Y. Almalioglu, P. P. B. de Gusmao, C. Chen, K. Sun, N. Trigoni, and A. Markham, "Milliego: Single-chip mmwave radar aided egomotion estimation via deep sensor fusion," in *Proceedings of the 18th Conference on Embedded Networked Sensor Systems*, ser. SenSys '20. New York, NY, USA: Association for Computing Machinery, 2020, p. 109–122. [Online]. Available: https://doi-org.db.ub.oru.se/10.1145/3384419.3430776

[19] Y. Zhuang, B. Wang, J. Huai, and M. Li, "4d iriom: 4d imaging radar inertial odometry and mapping," *IEEE Robotics and Automation Letters*, vol. 8, no. 6, pp. 3246–3253, 2023.

[20] K. Koide, J. Miura, and E. Menegatti, "A portable three-dimensional lidar-based system for long-term and wide-area people behavior measurement," *International Journal of Advanced Robotic Systems*, vol. 16, 02 2019.

[21] M. Grupp, "evo: Python package for the evaluation of odometry and slam." https://github.com/MichaelGrupp/evo, 2017.

[22] A. Geiger, P. Lenz, and R. Urtasun, "Are we ready for autonomous driving? the kitti vision benchmark suite," in *Conference on Computer Vision and Pattern Recognition (CVPR)*, 2012.

[23] K. Ebadi, L. Bernreiter, H. Biggie, G. Catt, Y. Chang, A. Chatterjee, C. E. Denniston, S.-P. Deschênes, K. Harlow, S. Khattak, L. Nogueira, M. Palieri, P. Petráček, M. Petrlík, A. Reinke, V. Krátký, S. Zhao, A. akbar Agha-mohammadi, K. Alexis, C. Heckman, K. Khosoussi, N. Kottege, B. Morrell, M. Hutter, F. Pauling, F. Pomerleau, M. Saska, S. Scherer, R. Siegwart, J. L. Williams, and L. Carlone, "Present and future of slam in extreme underground environments," 2022, arXiv preprint.